Syntheses and Characterizations of Cyanido-bridged Dinuclear Ru-complexes and Their MMCT Properties in the One-electron Oxidation State①

LIU Yang[a, b, c] ZHU Xiao-Quan[b]
WU Xin-Tao[b] SHENG Tian-Lu[b②]

[a] (*College of Chemistry, Fuzhou University, Fuzhou* 350002, *China*)
[b] (*State Key Laboratory of Structural Chemistry, Fujian Institute of Research on the Structure of Matter, Chinese Academy of Sciences, Fuzhou* 350002, *China*)
[c] (*University of Chinese Academy of Sciences, Beijing* 100049, *China*)

ABSTRACT We have designed and synthesized a family of dinuclear cyanido-bridged complexes [PY5Me$_2$Ru(μ-CN)Ru(dppe)CpMe$_n$][PF$_6$]$_2$ (PY5Me$_2$ = 2,6-bis (1,1-bis(2-pyridyl)ethyl) pyridine, Cp = cyclopentadienyl, n = 0, **2**[PF6]$_2$; n = 1, **3**[PF6]$_2$; n = 5, **4**[PF6]$_2$) by using a mononuclear complex [PY5Me$_2$Ru(μ-CN)][PF$_6$] (**1**) as the precursor. All the three complexes have been fully characterized by including single-crystal X-ray diffraction analysis. The one-electron oxidation complexes **2**$^{3+}$, **3**$^{3+}$ and **4**$^{3+}$ obtained in situ all show a MMCT absorption band in the visible range. The MMCT energy increases as the redox potential of the N-terminal fragments decreases, and the redox potential decreases as the number of methyl groups on the cyclopentadiene of the cyanido-nitrogen coordinated Ru metal increases, supported by the TDF/TDDFT calculations.

Keywords: electron transfer, mixed-valence, metal to metal charge transfer (MMCT), cyanide bridge;
DOI: 10.14102/j.cnki.0254-5861.2011-3147

1 INTRODUCTION

The investigation on electron transfer process has attracted a lot of attention from chemists and physicists over the past decades[1-4], because understanding electron transfer process is very important in some critical issues such as designing artificial photosynthesis[5], exposing catalytic mechanisms[6], development of superconducting materials[4], design of molecular electronic devices[7, 8], etc. Mixed-valence (MV) complexes are ideal simple models for investigating electron transfer process[9-13]. Low-valent metals can be used as electron donors to transfer electrons to high-valent metal electron acceptor fragments. Using mixed valence model makes it easy to calculate the electron transfer rate and the activation energy of intervalence electron transfer[14, 15]. Among them, the investigation on dinuclear ruthenium is the most common[16-19], such as the Creutz-Taube ion[20]. Various bridges can be used to connect the electron donors and acceptors, such as pyrazine[20], alkyne[21-31], cyanide bridges[16, 32-54], naphthalene[55-58], the organic bridge with redox activity[59, 60] and even mononuclear metals with multiple coordination sites[50, 54]. To date, it has been investigated how electron transfer process is influenced by the distance between the two metals[30], the energy barrier of electron transfer[54] and the *cis*-/*trans*-configuration. Cyanide is a short-range and asymmetric linear bridging ligand. The cyanide C-terminal metal feeds back much stronger electrons to the C≡N anti-orbital through the dπ orbital than the cyanide N-terminal metal does. For this reason, the cyanide C-terminal metal is often used as electron-donor and the cyanide N-terminal metal as electron-acceptor. The metal center can effectively transfer electrons through the cyanide bridge. Therefore, cyanide bridge is often used as a bridging ligand to investigate the electron transfer process in asymmetric mixed-valence dinuclear compounds.

Received 22 February 2021; accepted 26 March 2021 (**CCDC 2058046, 2058103, 2058110 and 2058112 for 1~4, respectively**)
① We thank the National Science Foundation of China (21773243, 21973095) and the Strategic Priority Research Program of Chinese Academy of Sciences (XDB20010200) for financial support
② Corresponding author. Sheng Tian-Lu, E-mail: tsheng@fjirsm.ac.cn

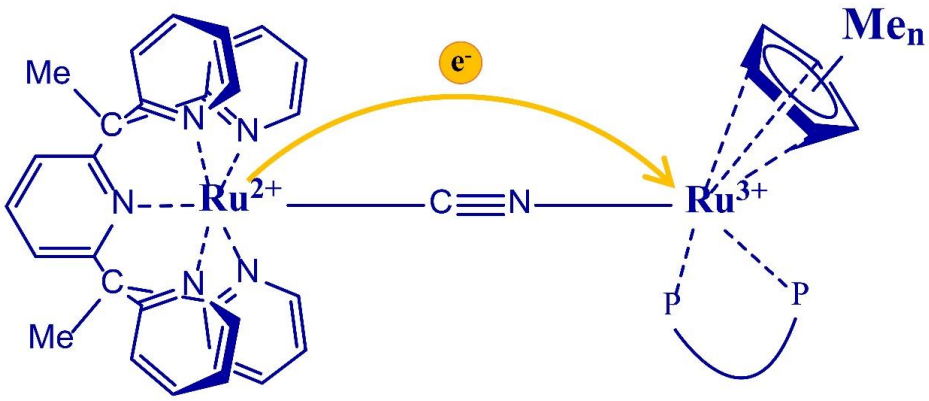

Fig. 1. Chemical structure of complexes 2^{3+} (n = 0), 3^{3+} (n = 1) and 4^{3+} (n = 5)

Our group has carried out a systematic study on the regulation of electron transfer in cyanide bridged mixed- valence compounds by different methods, such as changing the electron donating ability of ligands, cyanide bridge orientation, cis-trans isomerism and so on[49, 50, 53, 54]. In our previous studies, we found that changing the electron- donating ability of the ligand in the electron acceptor fragment has a more impact on the behavior of MMCT than in the electron-donor fragment[53]. To further investigate the influence of electron-acceptor fragment's electron-accepting ability on the behavior of MMCT, we have synthesized and characterized three complexes $[(PY5Me_2)Ru(\mu\text{-}CN)Ru\text{-}(dppe)CpMe_n]^{2+}$ ($\mathbf{2}^{2+}$, n = 0; $\mathbf{3}^{2+}$, n = 1; $\mathbf{4}^{2+}$, n = 5). As shown in Fig. 1, all the one-electron oxidation complexes $\mathbf{N}^{3+}$ (N = 2, 3, 4), which are obtained in situ by gradually adding cerium ammonium nitrate in acetonitrile solution of the $\mathbf{N}^{2+}$ complexes, exhibit a metal-to-metal charge transfer (MMCT) properties. The MMCT energy can be tuned by changing the number of methyl groups of cyclopentadiene located on the Ru center of the electron acceptor fragment, further supported by the time-dependent density functional theory (TD-DFT) calculations.

2 EXPERIMENTAL

2. 1 Physical measurements

Vario MICRO elemental analyzer was used to detect the element content (C, H and N). Infrared (IR) spectra were collected using KBr pellets on a PerkinElmer Spectrum. UV-vis-NIR absorption spectroscopy was collected with the PerkinElmer Lambda 365 UV-vis-NIR spectrophotometer. The cyclic voltammetry curve was measured under argon by V3-Studio with methylene chloride as the solvent and 0.1 M (Bu_4N) PF_6 as the promoting electrolyte at a scan rate of 100 mVs^{-1}. The electrolytic cell consists of glassy graphite as working electrode, platinum as counter electrode and Ag/AgCl as the reference electrode. Ferrocene was used to calibrate the potential. The single-crystal X-ray diffraction data for complexes **2** $[PF_6]_2$, **3** $[PF_6]_2$ and **4** $[PF_6]_2$ were collected on a Saturn 724^+ CCD diffractometer equipped with graphite-monochromatic Mo*Ka* (λ = 0.71073 Å) radiation at 293 K. Complex **1** (**PF_6**) was collected on a metal Jet D^{2+} diffractometer with graphite-monochromatic Ga*Kα* (λ = 1.3405 Å) radiation at 110 K. All structures were solved by intrinsic phasing methods using ShelXT-2018/3 and refined with ShelXL-2018/3[61], $OLEX_2$[62] program package. The SQUEEZE program in the PLATON software was used[63].

2. 2 Materials and synthesis

2. 2. 1 Materials

All operations were performed under argon atmosphere using standard Schlenk technology, unless otherwise specified. $PY5Me_2$[64], CpRu(dppe)Cl[65], CpMeRu(dppe)Cl[51] and $CpMe_5Ru(dppe)Cl$[66] were prepared by the previous literature. Methanol, ethanol and dichloromethane are 50 ppm super-dry solvents purchased from Adamas. All other raw materials were purchased commercially and used without further purification.

2. 2. 2 Synthesis

2. 2. 2. 1 Preparation of $PY5Me_2RuCl_2$

At room temperature, $RuCl_3 \cdot 3H_2O$ (1.0 g, 3.82 mmol) was added to 300 mL of anhydrous ethanol. The mixture was

refluxed at 88 °C for 6 hours, and then cooled to room temperature, to which $PY5Me_2$ (1.7 g, 3.83 mmol) in 50 mL ethanol was added. The mixture was refluxed at 88 °C for 48 hours, cooled to room temperature and filtered to remove the precipitate. The filtrate was rotary evaporated to remove the solvent to obtain a pale yellow crude product, which was recrystallized with ethanol to obtain 1.4 g of pure product with a yield of 57.5%.

2. 2. 2. 2 Preparation of [PY5Me$_2$RuCN][PF$_6$], 1[PF$_6$]

At room temperature, 10 equivalents of KCN (1.02 g, 15.7 mmol) were added to an aqueous solution of $PY5Me_2RuCl_2$ (1.0 g, 1.57 mmol). The mixture was refluxed at 110 °C for 2 hours, then cooled to room temperature, and an excess of NH_4PF_6 was added, resulting in a light green precipitate. The precipitate was filtered and dried in vacuum, giving 1.02 g light green product of **1**[PF_6] (yield 90.8%). The yellow crystals of **1**[PF_6] suitable for X-ray diffraction single-crystal structure analysis were obtained by slow diffusion of anhydrous ether into the DMF solution of **1**[PF_6] (75 mg, yield 81%).

Anal. Calcd. (%) for $C_{30}H_{25}N_6F_6PRu\cdot 2H_2O$: C, 47.97; H, 3.86; N, 11.19. Found (%): C, 47.69/47.85; H, 4.02/4.04; N, 11.00/11.01. IR (ν_{CN}, KBr pellet): 2077 cm^{-1}.

2. 2. 2. 3 Preparation of [PY5Me$_2$Ru^{II}CNRu^{II}(dppe)Cp][PF$_6$]$_2$, 2[PF$_6$]$_2$

At room temperature, the compound $PY5Me_2RuCN$ [PF_6] (50 mg, 0.07 mmol) was added to 1 equivalent of CpRu(dppe)Cl (42 mg, 0.07 mmol) in methanol (10 mL). The mixture was refluxed for 24 hours and cooled to room temperature. An excess of NH_4PF_6 was added and stirred for ten minutes to obtain a red precipitate. This precipitate was filtered and washed with a small amount of methanol and ether, giving the product of **2**[PF_6]$_2$. The yellow crystals of **2**[PF_6]$_2$ suitable for X-ray diffraction single-crystal structure analysis were obtained by slow diffusion of anhydrous ether into the dichloromethane solution of **2**[PF_6]$_2$ (69 mg, yield 75%).

Anal. Calcd. (%) for $C_{61}H_{54}F_{12}N_6P_4Ru_2\cdot CH_3CN$: C, 51.30; H, 3.89; N, 6.69. Found (%): C, 50.78; H, 3.81; N, 6.90. IR (ν_{CN}, KBr pellet): 2093 cm^{-1}.

2. 2. 2. 4 Preparation of [PY5Me$_2$Ru^{II}CNRu^{II}(dppe)MeCp][PF$_6$]$_2$, 3[PF$_6$]$_2$

At room temperature, the compound $PY5Me_2RuCN$ [PF_6] (50 mg, 0.07 mmol) was added to 1 equivalent of Cp^1Ru(dppe)Cl (43 mg, 0.07 mmol) in methanol (10 mL). The mixture was refluxed for 24 hours and cooled to room temperature. Then an excess of NH_4PF_6 was added and stirred for ten minutes to obtain a red precipitate which was filtered and washed with a small amount of methanol and ether, giving the product of **3**[PF_6]$_2$. The yellow crystals of **3**[PF_6]$_2$ suitable for X-ray diffraction single-crystal structure analysis were obtained by slow diffusion of anhydrous ether into the dichloromethane solution of **3**[PF_6]$_2$ (75 mg, yield 81%).

Anal. Calcd. (%) for $C_{62}H_{56}F_{12}N_6P_4Ru_2\cdot CH_3CN$: C, 51.89; H, 3.99; N, 6.62. Found (%): C, 52.10/51.49; H, 3.98/4.01; N, 6.64/6.56. IR (ν_{CN}, KBr pellet): 2091 cm^{-1}.

2. 2. 2. 5 Preparation of [PY5Me$_2$Ru^{II}CNRu^{II}(dppe)Me$_5$Cp][PF$_6$]$_2$, 4[PF$_6$]$_2$

At room temperature, the compound $PY5Me_2RuCN$ [PF_6] (50 mg, 0.07 mmol) was added to 1 equivalent of Cp^5Ru (dppe) Cl (47 mg, 0.07 mmol) in methanol (10 mL), and the resulting mixture was refluxed for 24 hours and cooled to room temperature. An excess of NH_4PF_6 was added and stirred for ten minutes to obtain a red precipitate. The precipitate was filtered and washed with a small amount of methanol and ether, giving the product of **4**[PF_6]$_2$. The yellow crystals of **4**[PF_6]$_2$ suitable for X-ray diffraction single-crystal structure analysis were obtained by slow diffusion of anhydrous ether into the dichloromethane solution of **4**[PF_6]$_2$ (55 mg, yield 53%).

Anal. Calcd. (%) for $C_{66}H_{64}F_{12}N_6P_4Ru_2\cdot H_2O$: C, 52.38; H, 4.37; N, 5.55. Found (%): C, 52.75/52.62; H, 4.78/4.89; N, 5.63/5.53. IR (ν_{CN}, KBr pellet): 2067 cm^{-1}.

3 RESULTS AND DISCUSSION

3. 1 X-ray structure determination

X-ray crystal structures of complexes **1**[PF_6] and **2**[PF_6]$_2$~**4**[PF_6]$_2$ are shown in Fig. 2. The crystallographic data are summarized in Table 1. The space groups of compounds **1**[PF_6], **2**[PF_6]$_2$, **3**[PF_6]$_2$ and **4**[PF_6]$_2$ are *Pbcm*, $P\bar{1}$, $P2_1/m$ and $P2_1/n$, respectively. For dinuclear complexes **2**[PF_6]$_2$~**4**[PF_6]$_2$, the structures of their anions are similar. In the structure of each anion, the Ru(1) and Ru(2) centers are bridged through the cyanide ligand, and are six- and four-coordinated by five N atoms from the $PY5Me_2$ ligand and one cyanido-carbon atom and by cyclopentadiene, one cyanido-nitrogen atom and the two P atoms from the dppe ligand, respectively. Some selected bond lengths and angles are listed in Table 2. The Ru(1)-C(1) ≡ N(1)-Ru(2) arrangements of all dinuclear Ru complexes are close to a linearity with bond angles of almost 180º. For compounds **2** and **3**, the

bond lengths and angles are very similar, but compound **4** has undergone significant changes. First, the cyanide bond length increases due to the increase of electrons on the Ru(2) *d* orbital feedback to the cyanide π^* orbital, which reduces the cyanide bond level. The change trend of cyanide length is consistent with the results of the cyclic voltammetry and the infrared spectroscopy. Second, the bond lengths of Ru(1)–N(av.), Ru(2)–P(av.) and Ru–Cp become longer, which may be caused by the greater steric hindrance of the ligand as the methyl group increases. This indicates that the change of bond lengths between the metal center and ligand of such compounds not only depends on the electronic effect of the ligand, but also is affected by the steric effect of the ligand.

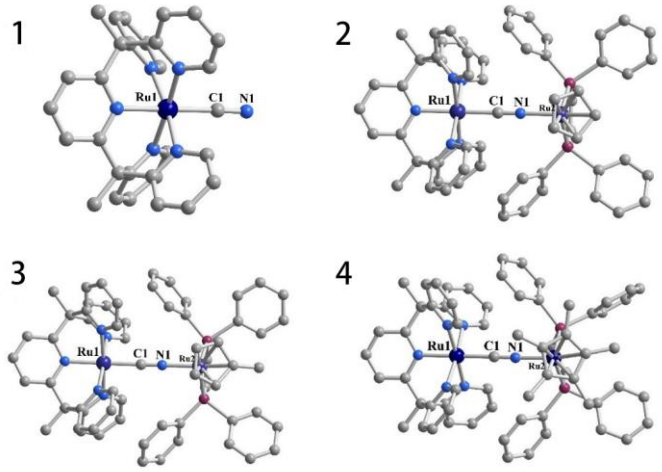

Fig. 2. X-ray crystal structures of complexes 1~4 ($[PF_6]^-$ ions, hydrogen atoms, acetonitrile and dichloromethane molecules have been removed for easy observation). Ru, dark blue; N, blue; P, wine red; C, grey

Table 1. Test Condition, Structure Refine and Crystallographic Data for Compounds 1[PF_6], 2[PF_6]$_2$, 3[PF_6]$_2$ and 4[PF_6]$_2$

Complex	1[PF_6]	2[PF_6]$_2$	3[PF_6]$_2$	4[PF_6]$_2$·CH_2Cl_2
Empirical formula	$C_{30}H_{24.6}F_6N_6PRu$	$C_{65}H_{61}Cl_4F_{12}N_7P_4R$	$C_{62}H_{56}F_{12}N_6P_4Ru_2$	$C_{67}H_{66}Cl_2F_{12}N_6P_4R$
Formula weight	715.20	1636.02	1439.07	1580.17
Temperature/K	293(2)	293(2)	100.00(10)	293(2)
Crystal system	Orthorhombic	Triclinic	Monoclinic	Monoclinic
Space group	*Pbcm*	$P\bar{1}$	$P2_1/m$	$P2_1/n$
a/Å	9.02510(10)	11.1761(14)	11.4028(4)	14.3242(4)
b/Å	17.5909(3)	14.0233(7)	23.5113(6)	24.0896(6)
c/Å	21.2449(4)	23.9935(7)	13.4498(6)	21.0103(5)
α/°	90	86.469(3)	90	90
β/°	90	89.574(3)	113.502(5)	102.308(2)
γ/°	90	66.624(4)	90	90
Volume/Å^3	3372.83(9)	3444.6(3)	3306.7(2)	7083.3(3)
Z	4	2	2	4
ρ_{calcg}/cm^3	1.408	1.577	1.445	1.482
μ/mm^{-1}	0.574	0.765	3.480	0.668

To be continued

F(000)	1438.0	1648.0	1452.0	3200.0
Crystal size/mm^3	0.32×0.11×0.08	0.31×0.28×0.20	0.31×0.15×0.11	0.11×0.11×0.08
Radiation	MoKα (λ = 0.71073)	MoKα (λ = 0.71073)	Metaljet (λ = 1.3405)	MoKα (λ = 0.71073)
2θ range/°	4.632 to 52.732	3.5 to 52.742	6.23 to 121.62	3.366 to 52.744
Index ranges	−11≤h≤11, −21≤k≤21, −26≤l≤26	−13≤h≤13, −17≤k≤17, −29≤l≤29	−14≤h≤14, −27≤k≤30, −17≤l≤17	−17≤h≤17, −30≤k≤30, −26≤l≤26
Reflections collected	46444	48982	47679	106915
Independent reflections	3442	14083	7671	14482
Da-	3442/6/223	14083/0/850	7671/64/455	14482/0/845
Goodness-of-fit on F^2	1.099	1.042	1.080	1.035
Final R indexes(I>2σ(I))	R=0.0311, R=0.0778	R=0.0920, R=0.2372	R=0.0376, wR=0.1006	R=0.0550, wR=0.1510
Final R indexes (all data)	R=0.0332,wR=0.0790	R=0.1237,wR=0.2748	R=0.0442, wR=0.1056	R=0.0697, wR=0.1617

Table 2. Selected Bond Lengths (Å) and Bond Angles (°) for Compounds 1~4

	1[PF_6]	**2**[PF_6]$_2$	**3**[PF_6]$_2$	**4**[PF_6]$_2$
Ru(1)–C(1)	2.013(3)	1.990(6)	1.993(4)	2.026(4)
C(1)–N(1)	1.134(4)	1.144(8)	1.148(5)	1.162(5)
N(1)–Ru(2)		2.039(5)	2.055(3)	2.089(3)
Ru(1)–N(av.)	2.077(18)	2.076(5)	2.083(4)	2.087(4)
Ru(2)–P(av.)		2.2661(18)	2.2697(7)	2.3095(11)
Ru(2)–Cp		1.864	1.857	1.891
Ru(1)···Ru(2)		5.155	5.191	5.277
Ru(1)–C(1)–N(1)	178.3(3)	174.0(6)	175.4(3)	178.1(4)
Ru(2)–N(1)–C(1)		175.0(5)	178.7(3)	177.5(3)

3. 2 Electrochemistry

The cyclic voltammetry of the four compounds in dichloromethane all showed one reversible redox wave. The results are shown in Fig. 3 and Table 2. The cyclic voltammetry of complexes **2**[PF_6]$_2$, **3**[PF_6]$_2$ and **4**[PF_6]$_2$ each shows one reversible redox wave at 0.342, 0.267 and 0.234 V, respectively, which could be attributed to $CpMe_n(dppe)Ru^{II}$/$CpMe_n(dppe)Ru^{III}$ and is higher than the similar monomer[67] based on the previous paper[53]. The redox wave of the mononuclear complex **1**[PF_6]$_2$ exhibits one redox wave assigned to $(PY5Me_2)Ru^{II}$/$(PY5Me_2)Ru^{III}$. However, the same redox wave for $(PY5Me_2)Ru^{II}$/$(PY5Me_2)Ru^{III}$ in the three dinuclear complexes was not observed, which may be due to its too higher potential position. From Table 3, it can be found that with the increase of the number of methyl groups on cyclopentadiene the redox wave position moves to a lower potential from **2**[PF_6]$_2$ and **3**[PF_6]$_2$ to **4**[PF_6]$_2$.

Table 3. Electrochemical Data (vs Cp_2Fe+/0) for Complexes 1~4 in 0.10 M DCM Solution of Bu_4NPF_6 at a Scan Rate of 100 mV·s^{-1}

Complex	L	$E_{1/2}$/V
1[PF_6]		0.59
2[PF_6]$_2$	Cp	0.342
3[PF_6]$_2$	CpMe	0.267
4[PF_6]$_2$	$CpMe_5$	0.234

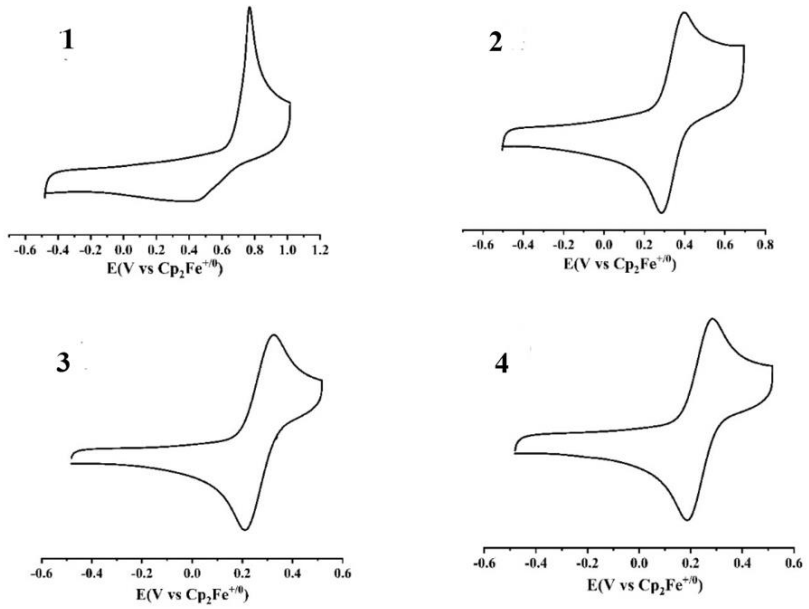

Fig. 3. Cyclic voltammograms of 1^{2+}~4^{2+} in a 0.10M dichloromethane solution of Bu_4NPF_6 at a scan rate of 100 mV·s^{-1} vs $(Cp_2Fe)^{+/0}$

3. 3 IR spectroscopy

Infrared spectroscopy is an excellent way to characterize cyanide bridged compounds. The contraction vibration of cyanide is easy to observe in infrared spectroscopy, and the cyanide stretching ν(CN) position can help us judge the connection rigidity and electrons feedback situation of the compounds. Compared with the position of the terminal cyanide signal of the mononuclear compound $[PY5Me_2RuCN]^+$ (2077 cm^{-1}), the position of the bridged cyanide band of the dinuclear compounds $\mathbf{2}^{2+}$ (2093 cm^{-1}) and $\mathbf{3}^{2+}$ (2091 cm^{-1}) has a blue shift due to the rigid restriction of the cyanide N-coordinated Ru on the movement of the bridging cyanide. But for compound $\mathbf{4}^{2+}$, the pentamethylcyclopentadiene ligand has a stronger electron-donating ability. It promotes the transfer of *d* orbital electron of the nitrogen-terminal Ru fragment to the π anti-bond orbital of the cyanide bridge to form a feedback π bond, which reduces the cyanide energy level and results in the absorption peak redshift. With the enhancement of the electron-donating ability of the ligand on the C-terminal metal, the redshift of the cyanide vibration frequency is often observed, but it is rare to reduce the cyanide vibration energy through the feedback electron from the N-terminal metal.

Table 4. CN Stretching Frequencies for Complexes $1(PF_6)$~$4(PF_6)_2$

Complex	L	ν(cm^{-1})
1[PF_6]		2077
2[PF_6]$_2$	Cp	2093
3[PF_6]$_2$	CpMe	2091
4[PF_6]$_2$	$CpMe_5$	2067

3. 4 UV-VIS-NIR spectroscopy

UV-VIS-NIR absorption spectroscopy is the most effective method for studying electron transfer. According to the strongest absorption position, absorption intensity and half-width of the MMCT absorption peak, the strength of the electron transfer of the compound can be investigated. In order to study the influence of the electron-donating ability of the acceptor terminal ligand on the MMCT, we used the acetonitrile solution of cerium ammonium nitrate to gradually oxidize the three dinuclear compounds to obtain mixed-valence compounds in situ. Their absorption spectra were measured, as shown in Figs. 4 and 5. The absorption

peak from 27500 cm^{-1} to 22000 cm^{-1} for each of the mixed-valence compounds $\mathbf{2}^{3+}$, $\mathbf{3}^{3+}$ and $\mathbf{4}^{3+}$ obtained in situ is attributed to the metal-to-ligand electron transfer (MLCT) from Ru^{2+} to the $PY5Me_2$ ligand[68], and the new absorption peak from 16000 cm^{-1} to 9000 cm^{-1} is attributed to the metal-to-metal electron transfer (MMCT)[53]. For MLCT absorption peaks, the maxima absorption peaks of the three compounds $\mathbf{2}^{2+}$, $\mathbf{3}^{2+}$ and $\mathbf{4}^{2+}$ before oxidation are basically the same, all at about 25000 cm^{-1}. After one-electron oxidation, it can be observed that the positions of the MLCT maxima absorption peaks of the three dinuclear mixed valence Ru compounds $\mathbf{2}^{3+}$, $\mathbf{3}^{3+}$ and $\mathbf{4}^{3+}$each exhibits a significant blue shift, and the absorption intensity is also significantly weakened. This is because that from $\mathbf{2}^{2+}$, $\mathbf{3}^{2+}$ and $\mathbf{4}^{2+}$ to $\mathbf{2}^{3+}$, $\mathbf{3}^{3+}$ and $\mathbf{4}^{3+}$ the electron-donating ability of Ru^{II} in the $(PY5Me_2)Ru^{II}$ fragment weakens due to the electron withdraw effect of the $CpMe_n(dppe)Ru^{III}$.

For the MMCT absorption peak, with the increase of the electron-donating ability of the substituted group from Cp, CpMe to $CpMe_5$, the MMCT absorption peaks of the three mixed-valence compounds each shows a blue shift (10953 cm^{-1} for $\mathbf{2}^{3+}$, 11274 cm^{-1} for $\mathbf{3}^{3+}$ and 11442 cm^{-1} for $\mathbf{4}^{3+}$), and the absorption intensity increases (2125M^{-1} cm^{-1}→2324 M^{-1} cm^{-1}→2786 M^{-1} cm^{-1}). This is because that the electron-accepting ability of Ru^{III} in the $CpMe_n(dppe)Ru^{III}$ fragment decreases as the electron-donating ability increases from Cp, CpMe to $CpMe_5$, resulting in the increase of the Ru^{II}→Ru^{III} MMCT energy from $\mathbf{2}^{3+}$, $\mathbf{3}^{3+}$ to $\mathbf{4}^{3+}$, strongly supported by the TD-DFT calculation.

The electronic coupling constant H_{ab} of complexes $\mathbf{2}^{3+}$~$\mathbf{4}^{3+}$ was calculated using the Hush-Mullikan equation (Eq. 1)[9], with the results listed in Table 5. In the equation, $\nu_{1/2}$ is the bandwidth at half-intensity of the MMCT band maximum ν_{max}, and ε_{max} and r_{AB} represent the molar extinction coefficient and the through space intermetallic distance, respectively. As shown in Table 5, the electronic coupling constant H_{ab} gradually increases from $\mathbf{2}^{3+}$, $\mathbf{3}^{3+}$ to $\mathbf{4}^{3+}$. This may be understood by the fact that as the number of methyl groups of Cp increases the mixed valence state [Ru^{II}-CN-Ru^{III}] becomes more and more stable, resulting in the more and more MMCT energy from [Ru^{II}-CN-Ru^{III}] to [Ru^{III}-CN-Ru^{II}] from $\mathbf{2}^{3+}$, $\mathbf{3}^{3+}$ to $\mathbf{4}^{3+}$, and the H_{ab} increases correspondingly. According to the calculation results, the one-electron oxidation products $\mathbf{2}^{3+}$, $\mathbf{3}^{3+}$ and $\mathbf{4}^{3+}$ belong to the class II mixed valence compounds.

$$H_{AB}=2.06\times10^{-2}\frac{\left(\lambda_{max}\cdot\varepsilon_{max}\cdot\Delta V_{1/2}\right)^{1/2}}{r_{AB}} \qquad \text{Eq. 1}$$

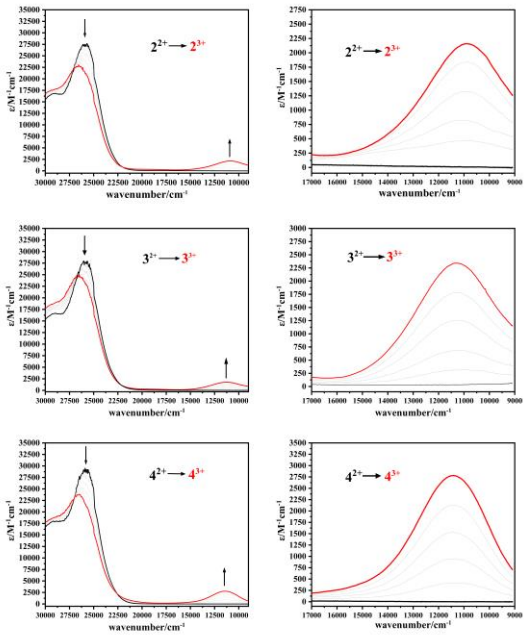

Fig. 4. UV-Vis-NIR absorption spectra of complexes 2~4 oxidized by the addition of ammonium ceric nitrate in acetonitrile

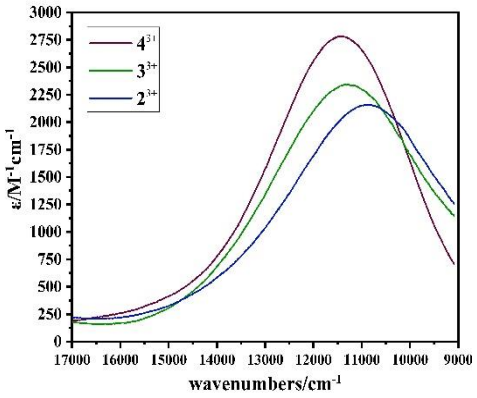

Fig. 5. MMCT absorption spectra of complexes 2~4 oxidized by adding ammonium ceric nitrate in acetonitrile

Table 5. MMCT Transition Energies and Electronic Coupling Constant for All the Mixed-valence Complexes

Complex	λ_{max}/cm^{-1}	ε_{max}/M^{-1}·cm^{-1}	H_{ab}
2[PF$_6$]$_3$	10953	2125	1235
3[PF$_6$]$_3$	11274	2324	1293
4[PF$_6$]$_3$	11442	2786	1479

3. 5 DFT/TDDFT calculations

To continue studying the influence of electron acceptor orbital changes on the properties of MMCT, we performed TD-DFT calculations using B3LYP/lanl2dz[69, 70] for the three MV compounds. As shown in Table 6, the spin electron density of the three MV compounds is mainly localized on Ru^{III}, further indicating that the single-electron oxidation products of the three compounds belong to the class Ⅱ mixed-valence compounds. Due to the decrease of electron-accepting ability of the acceptor fragments from $\mathbf{2}^{3+}$, $\mathbf{3}^{3+}$ to $\mathbf{4}^{3+}$, the $Ru^{II} \rightarrow Ru^{III}$ MMCT gets to be more difficult, resulting in an increase of the spin electron density on the acceptor metal center. For MMCT, the calculation results are basically consistent with the experimental data, as shown in Table 7. The metal donor HOMO orbitals and acceptor LUMO orbitals of the three MV compounds are shown in Fig. 6. The major contribution for the MMCT absorption band of complex $\mathbf{2}^{3+}$ comes from molecular orbital 248B to 251B. For compound $\mathbf{3}^{3+}$, the MMCT absorption peak is mainly derived from molecular orbital 252B to 255B. For compound $\mathbf{4}^{3+}$, the MMCT absorption peak mainly comes from the molecular orbitals from 268B to 271B. The LUMO orbitals of the three compounds are almost localized on Ru^{3+}, while the HOMO ones are localized on Ru^{2+}, which indicates that the three compounds all belong to the class II mixed-valence compounds, consistent with the measured UV-Vis-NIR absorption spectral results.

Table 6. Mulliken Spin Density of Mixed-valence Species

	Ru1	Ru2
$\mathbf{2}^{3+}$	0.072983	0.761033
$\mathbf{3}^{3+}$	0.072559	0.779743
$\mathbf{4}^{3+}$	0.042988	0.832436

Table 7. Comparison of the Measured and the Calculated MMCT Energies of $\mathbf{2}^{3+}$, $\mathbf{3}^{3+}$ and $\mathbf{4}^{3+}$

Complex	Measured (cm^{-1})	Calculated (cm^{-1})
$\mathbf{2}^{3+}$	10953	12469
$\mathbf{3}^{3+}$	11274	12407
$\mathbf{4}^{3+}$	11442	13755

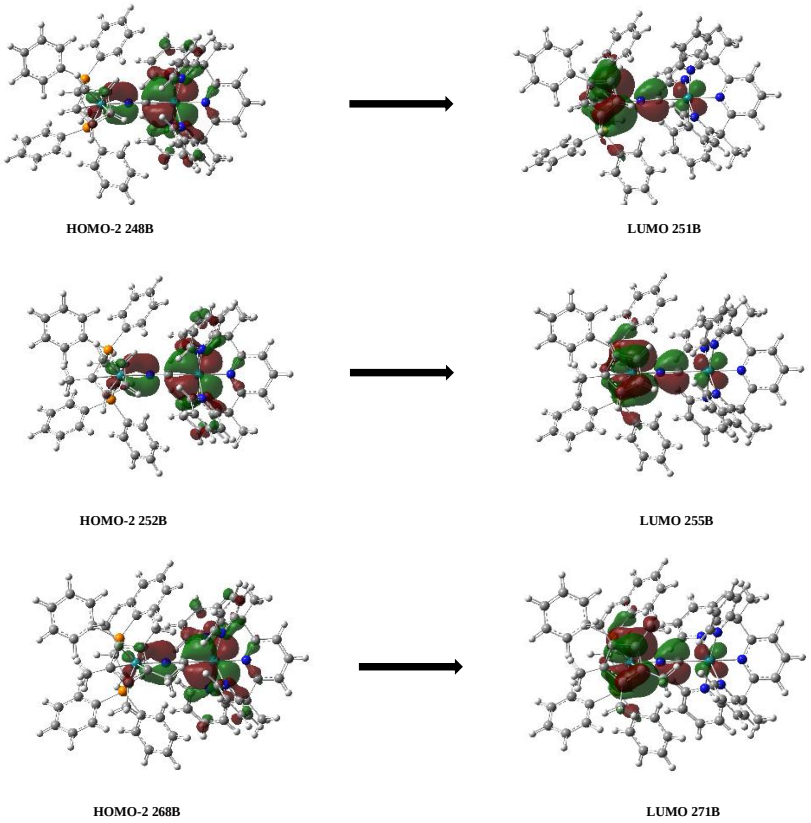

Fig. 6. Molecular orbital diagrams of HOMO-2 (248B) and LUMO (251B) for 2 (above), HOMO-2 (252B) and LUMO (255B) for 3 (middle), HOMO-2 (268B) and LUMO (271B) for 4 (bottom). The isosurface value is 0.02 au

4 CONCLUSION

In summary, we have synthesized and characterized a mononuclear Ru fragment and three cyanido-bridged dinuclear Ru compounds $\mathbf{2}^{2+}$, $\mathbf{3}^{2+}$ and $\mathbf{4}^{2+}$. All one-electron oxidation complexes $\mathbf{2}^{3+}$, $\mathbf{3}^{3+}$ and $\mathbf{4}^{3+}$ obtained in situ show a MMCT absorption band in the NIR range. The MMCT energy increases as the number of methyl groups on the cyclopentadiene of the cyanido-nitrogen coordinated Ru metal increases, supported by the DFT/TDDFT calculations. Furthermore, the UV-vis-NIR absorption spectra and TDDFT calculations show that all the single-electron oxidation compounds belong to class Ⅱ mixed-valence compounds. This work shows that slight modifications to the ligand on the N-terminal metal center can tune the MMCT properties of the mixed valence compounds.

REFERENCES

(1) Marcus, R. A. Chemical and electrochemical electron-transfer theory. *Annu. Rev. Phys. Chem.* **1964**, 15, 155–196.

(2) Hush, N. S. Homogeneous and heterogeneous optical and thermal electron transfer. *Electrochim. Acta* **1968**, 13, 1005–1023.

(3) Rafiq, S.; Scholes, G. D. From fundamental theories to quantum coherences in electron transfer. *J. Am. Chem. Soc.* **2019**, 141, 708–722.

(4) Aubrey, M. L.; Wiers, B. M.; Andrews, S. C.; Sakurai, T.; Reyes-Lillo, S. E.; Hamed, S. M.; Yu, C. J.; Darago, L. E.; Mason, J. A.; Baeg, J. O.; Grandjean, F.; Long, G. J.; Seki, S.; Neaton, J. B.; Yang, P.; Long, J. R. Electron delocalization and charge mobility as a function of reduction in a metal-organic framework. *Nat. Mater.* **2018**, 17, 625–632.

(5) Levanon, H.; Norris, J. R. The photoexcited triplet state and photosynthesis. *Chem. Rev.* **1978**, 78, 185–198.

(6) Kochi, J. K. Electron-transfer mechanisms for organometallic intermediates in catalytic reactions. *Acc. Chem. Res.* **2002**, 7, 351–360.

(7) Nitzan, A.; Ratner, M. A. Electron transport in molecular wire junctions. *Science* **2003**, 300, 1384–9.

(8) Wenger, O. S. Photoswitchable mixed valence. *Chem. Soc. Rev.* **2012**, 41, 3772–9.

(9) Heckmann, A.; Lambert, C. Organic mixed-valence compounds: a playground for electrons and holes. *Angew Chem. Int. Ed. Engl.* **2012**, 51, 326–92.

(10) Kang, M. T.; Meng, M.; Tan, Y. N.; Cheng, T.; Liu, C. Y. Tuning the electronic coupling and electron transfer in Mo2 donor-acceptor systems by variation of the bridge conformation. *Chemistry* **2016**, 22, 3115–26.

(11) Zhu, G. Y.; Meng, M.; Tan, Y. N.; Xiao, X.; Liu, C. Y. Electronic coupling between two covalently bonded dimolybdenum units bridged by a naphthalene group. *Inorg. Chem.* **2016**, 55, 6315–22.

(12) Cheng, T.; Xiao, X.; Zhang, L.; Liu, C. Y.; Wang, L. L.; Meng, M.; Zhao, F.; Wang, H.; Ji, L. N. Photoinduced delta electron transfer in phenylene bridged Mo2 dimers. *Phys. Chem. Chem. Phys.* **2017**, 19, 1740–1745.

(13) Zhu, G. Y.; Qin, Y.; Meng, M.; Mallick, S.; Gao, H.; Chen, X.; Cheng, T.; Tan, Y. N.; Xiao, X.; Han, M. J.; Sun, M. F.; Liu, C. Y. Crossover between the adiabatic and nonadiabatic electron transfer limits in the landau-zener model. *Nat. Commun.* **2021**, 12, 456.

(14) Lancaster, K.; Odom, S. A.; Jones, S. C.; Thayumanavan, S.; Marder, S. R.; Bredas, J. L.; Coropceanu, V.; Barlow, S. Intramolecular electron-transfer rates in mixed-valence triarylamines: measurement by variable-temperature ESR spectroscopy and comparison with optical data. *J. Am. Chem. Soc.* **2009**, 131, 171–23.

(15) Slenkamp, K. M.; Lynch, M. S.; Van Kuiken, B. E.; Brookes, J. F.; Bannan, C. C.; Daifuku, S. L.; Khalil, M. Investigating vibrational anharmonic couplings in cyanide-bridged transition metal mixed valence complexes using two-dimensional infrared spectroscopy. *J. Chem. Phys.* **2014**, 140, 084505.

(16) Oviedo, P. S.; Pieslinger, G. E.; Cadranel, A.; Baraldo, L. M. Exploring the localized to delocalized transition in non-symmetric bimetallic ruthenium polypyridines. *Dalton Trans.* **2017**, 46, 15757–15768.

(17) Tang, J. H.; Shao, J. Y.; He, Y. Q.; Wu, S. H.; Yao, J.; Zhong, Y. W. Transition from a metal-localized mixed-valence compound to a fully delocalized and bridge-biased electrophore in a ruthenium-amine-ruthenium tricenter system. *Chemistry* **2016**, 22, 10341–5.

(18) Zhong, Y. W.; Gong, Z. L.; Shao, J. Y.; Yao, J. Electronic coupling in cyclometalated ruthenium complexes. *Coord. Chem. Rev.* **2016**, 312, 22–40.

(19) Shao, J. Y.; Gong, Z. L.; Zhong, Y. W. Bridged cyclometalated diruthenium complexes for fundamental electron transfer studies and multi-stage redox switching. *Dalton Trans.* **2018**, 47, 23–29.

(20) Creutz, C.; Taube, H. Direct approach to measuring the franck-condon barrier to electron transfer between metal ions. *J. Am. Chem. Soc.* **1969**, 91, 3988–3989.

(21) Field, L. D.; Turnbull, A. J.; Turner, P. Acetylide-bridged organometallic oligomers via the photochemical metathesis of methyl-iron(II) complexes. *J. Am. Chem. Soc.* **2002**, 124, 3692–702.

(22) Venkatesan, K.; Blacque, O.; Berke, H. Organometallic manganese complexes as scaffolds for potential molecular wires. *Dalton Trans.* **2007**, 1091–100.

(23) Olivier, C.; Kim, B.; Touchard, D.; Rigaut, S. Redox-active molecular wires incorporating ruthenium(II) σ-arylacetylide complexes for molecular electronics. *Organometallics* **2008**, 27, 509–518.

(24) Benameur, A.; Brignou, P.; Di Piazza, E.; Hervault, Y. M.; Norel, L.; Rigaut, S. Redox-active ruthenium(II) σ-arylacetylide wires for molecular electronics incorporating insulating chains. *New J. Chem.* **2011**, 35.

(25) Luo, L.; Benameur, A.; Brignou, P.; Choi, S. H.; Rigaut, S.; Frisbie, C. D. Length and temperature dependent conduction of ruthenium-containing redox-active molecular wires. *J. Phys. Chem. C* **2011**, 115, 19955–19961.

(26) Egler-Lucas, C.; Blacque, O.; Venkatesan, K.; Lopez-Hernandez, A.; Berke, H. Dinuclear and mononuclear chromium acetylide complexes. *Eur. J. Inorg. Chem.* **2012**, 2012, 1536–1545.

(27) Lissel, F.; Fox, T.; Blacque, O.; Polit, W.; Winter, R. F.; Venkatesan, K.; Berke, H. Stepwise construction of an iron-substituted rigid-rod molecular wire: targeting a tetraferra-tetracosa-decayne. *J. Am. Chem. Soc.* **2013**, 135, 4051–60.

(28) Lissel, F.; Blacque, O.; Venkatesan, K.; Berke, H. Structural and electronic variations of sp/sp^2 carbon-based bridges in di- and trinuclear redox-active iron complexes bearing Fe(diphosphine)2x (x = i, ncs) moieties. *Organometallics* **2015**, 34, 408–418.

(29) Lissel, F.; Schwarz, F.; Blacque, O.; Riel, H.; Lörtscher, E.; Venkatesan, K.; Berke, H. Organometallic single-molecule electronics: tuning electron transport through x(diphosphine)2FeC4Fe(diphosphine)2x building blocks by varying the Fe-X-Au anchoring scheme from coordinative to covalent. *J. Am. Chem. Soc.* **2014**, 136, 14560–14569.

(30) Zheng, Q.; Hampel, F.; Gladysz, J. A. Longitudinally extended molecular wires based upon PtC≡CC≡CC≡C repeat units: iterative syntheses of functionalized linear PtC8Pt, PtC8PtC8Pt, and PtC8PtC8PtC8Pt assemblies. *Organometallics* **2004**, 23, 589–5899.

(31) Semenov, S. N.; Blacque, O.; Fox, T.; Venkatesan, K.; Berke, H. Electronic communication in dinuclear C(4)-bridged tungsten complexes. *J. Am. Chem. Soc.* **2010**, 132, 3115–27.

(32) Nihei, M.; Ui, M.; Yokota, M.; Han, L.; Maeda, A.; Kishida, H.; Okamoto, H.; Oshio, H. Two-step spin conversion in a cyanide-bridged ferrous square. *Angew Chem. Int. Ed. Engl.* **2005**, 44, 6484–7.

(33) Nihei, M.; Sekine, Y.; Suganami, N.; Nakazawa, K.; Nakao, A.; Nakao, H.; Murakami, Y.; Oshio, H. Controlled intramolecular electron transfers in cyanide-bridged molecular squares by chemical modifications and external stimuli. *J. Am. Chem. Soc.* **2011**, 133, 3592–600.

(34) Hoshino, N.; Iijima, F.; Newton, G. N.; Yoshida, N.; Shiga, T.; Nojiri, H.; Nakao, A.; Kumai, R.; Murakami, Y.; Oshio, H. Three-way switching in a cyanide-bridged [CoFe] chain. *Nat. Chem.* **2012**, 4, 921–6.

(35) Jiao, C. Q.; Meng, Y. S.; Yu, Y.; Jiang, W. J.; Wen, W.; Oshio, H.; Luo, Y.; Duan, C. Y.; Liu, T. Effect of intermolecular interactions on metal-to-metal charge transfer: a combined experimental and theoretical investigation. *Angew Chem. Int. Ed. Engl.* **20**19, 58, 17009–17015.

(36) Albores, P.; Slep, L. D.; Weyhermuller, T.; Baraldo, L. M. Fine tuning of the electronic coupling between metal centers in cyano-bridged mixed-valent trinuclear complexes. *Inorg. Chem.* **2004**, 43, 6762–73.

(37) Albores, P.; Slep, L. D.; Eberlin, L. S.; Corilo, Y. E.; Eberlin, M. N.; Benitez, G.; Vela, M. E.; Salvarezza, R. C.; Baraldo, L. M. From monomers to geometry-constrained molecules: one step further toward cyanide bridged wires. *Inorg. Chem.* **2009**, 48, 11226–35.

(38) Cadranel, A.; Albores, P.; Yamazaki, S.; Kleiman, V. D.; Baraldo, L. M. Efficient energy transfer via the cyanide bridge in dinuclear complexes containing Ru(II) polypyridine moieties. *Dalton Trans.* **2012**, 41, 5343–50.

(39) Pieslinger, G. E.; Albores, P.; Slep, L. D.; Coe, B. J.; Timpson, C. J.; Baraldo, L. M. Communication between remote moieties in linear Ru-Ru-Ru trimetallic cyanide-bridged complexes. *Inorg. Chem.* **2013**, 52, 2906–17.

(40) Pieslinger, G. E.; Albores, P.; Slep, L. D.; Baraldo, L. M. Class III delocalization in a cyanide-bridged trimetallic mixed-valence complex. *Angew Chem. Int. Ed. Engl.* **2014**, 53, 1293–6.

(41) Pieslinger, G. E.; Aramburu-Troselj, B. M.; Cadranel, A.; Baraldo, L. M. Influence of the electronic configuration in the properties of d6-d5 mixed-valence complexes. *Inorg. Chem.* **2014**, 53, 8221–9.

(42) Cadranel, A.; Oviedo, P. S.; Pieslinger, G. E.; Yamazaki, S.; Kleiman, V. D.; Baraldo, L. M.; Guldi, D. M. Trapping intermediate mlct states in low-symmetry {Ru(bpy)} complexes. *Chem. Sci.* **2017**, 8, 7434–7442.

(43) Cadranel, A.; Oviedo, P. S.; Albores, P.; Baraldo, L. M.; Guldi, D. M.; Hodak, J. H. Electronic energy transduction from {Ru(py)4} chromophores to Cr(III) luminophores. *Inorg. Chem.* **2018**, 57, 3042–3053.

(44) Aramburu-Troselj, B. M.; Oviedo, P. S.; Pieslinger, G. E.; Hodak, J. H.; Baraldo, L. M.; Guldi, D. M.; Cadranel, A. A hole delocalization strategy: photoinduced mixed-valence mlct states featuring extended lifetimes. *Inorg. Chem.* **2019**, 58, 10898–10904.

(45) Aramburu-Troselj, B. M.; Oviedo, P. S.; Ramirez-Wierzbicki, I.; Baraldo, L. M.; Cadranel, A. Inversion of donor-acceptor roles in photoinduced intervalence charge transfers. *Chem. Commun.* (*Camb*) **2019**, 55, 7659–7662.

(46) Oviedo, P. S.; Pieslinger, G. E.; Baraldo, L. M.; Cadranel, A.; Guldi, D. M. Coexistence of mlct excited states of different symmetry upon photoexcitation of a single molecular species. *J. Phys. Chem. C* **2019**, 123, 3285–3291.

(47) Dominguez, S. E.; Pieslinger, G. E.; Sanchez-Merlinsky, L.; Baraldo, L. M. Does geometry matter? Effect of the ligand position in bimetallic ruthenium polypyridine siblings. *Dalton Trans.* **2020**, 49, 4125–4135.

(48) Sheng, T.; Vahrenkamp, H. Long range metal-metal interactions along Fe−NC−Ru−CN−Fe chains. *Eur. J. Inorg. Chem.* **2004**, 2004, 1198–1203.

(49) Ma, X.; Lin, C. S.; Zhu, X. Q.; Hu, S. M.; Sheng, T. L.; Wu, X. T. An unusually delocalized mixed-valence state of a cyanidometal-bridged compound induced by thermal electron transfer. *Angew Chem. Int. Ed. Engl.* **2017**, 56, 1605–1609.

(50) Yang, Y. Y.; Zhu, X. Q.; Hu, S. M.; Su, S. D.; Zhang, L. T.; Wen, Y. H.; Wu, X. T.; Sheng, T. L. Different degrees of electron delocalization in mixed valence Ru-Ru-Ru compounds by cyanido-/isocyanido-bridge isomerism. *Angew Chem. Int. Ed. Engl.* **2018**, 57, 14046–14050.

(51) Li, S. H.; Liu, Y.; Yang, Y. Y.; Zhang, Y. X.; Xu, Q. D.; Hu, S. M.; Wu, X. T.; Sheng, T. L. Syntheses, crystal structures and mmct properties of cyanide-bridged binuclear Ru-Fe complexes. *Polyhedron* **2019**, 173.

(52) Su, S. D.; Zhu, X. Q.; Wen, Y. H.; Zhang, L. T.; Yang, Y. Y.; Lin, C. S.; Wu, X. T.; Sheng, T. L. A diruthenium-based mixed spin complex Ru2 (5+) (s = 1/2)-CN-Ru2 (5+) (s = 3/2). *Angew Chem. Int. Ed. Engl.* **2019**, 58, 15344–15348.

(53) Zhang, L. T.; Zhu, X. Q.; Hu, S. M.; Zhang, Y. X.; Su, S. D.; Yang, Y. Y.; Wu, X. T.; Sheng, T. L. Influence of ligand substitution at the donor and acceptor center on mmct in a cyanide-bridged mixed-valence system. *Dalton Trans.* **2019**, 48, 7809–7816.

(54) Yang, Y. Y.; Zhu, X. Q.; Launay, J. P.; Hong, C. B.; Su, S. D.; Wen, Y. H.; Wu, X. T.; Sheng, T. L. Electron transfer process in mixed valence compounds with low-lying energy bridge in different oxidation states. *Angew Chem. Int. Ed. Engl.* **2020**, 60, 4804–4814.

(55) Hatanaka, T.; Ohki, Y.; Kamachi, T.; Nakayama, T.; Yoshizawa, K.; Katada, M.; Tatsumi, K. Naphthalene and anthracene complexes sandwiched by two {(Cp*)Fe(I)} fragments: strong electronic coupling between the Fe(I) centers. *Chem. Asian J.* **2012**, 7, 1231–42.

(56) Schnöckelborg, E. M.; Hartl, F.; Langer, T.; Pöttgen, R.; Wolf, R. Redox-active, dinuclear sandwich compounds [Cp*Fe(μ-l)FeCp*] (l = naphthalene

and anthracene). *European Journal of Inorg. Chem.* **2012**, 2012, 1632–1638.

(57) Malberg, J.; Lupton, E.; Schnöckelborg, E. M.; de Bruin, B.; Sutter, J.; Meyer, K.; Hartl, F.; Wolf, R. Synthesis and electronic structure of dissymmetrical, naphthalene-bridged sandwich complexes [Cp′Fe(μ-c10h8)mcp*]*x* (*x* = 0, +1; m = Fe, Ru; Cp′ = η5-c5h2-1,2,4-tbu3; Cp* = η5-C5Me5). *Organometallics* **2013**, 32, 6040–6052.

(58) Herrmann, D.; Rodl, C.; de Bruin, B.; Hartl, F.; Wolf, R. Synthesis, electronic structure and redox properties of the diruthenium sandwich complexes [Cp*Ru(mu-C10H8)RuCp*](*x*) (*x* = 0, 1+; Cp* = C5Me5; C10H8 = naphthalene). *Dalton Trans.* **2018**, 47, 11058–11069.

(59) Ibanez, S.; Poyatos, M.; Peris, E. Mono and dimetallic pyrene-imidazolylidene complexes of iridium(III) for the deuteration of organic substrates and the C-C coupling of alcohols. *Dalton Trans.* **2016**, 45, 14154–9.

(60) Carter, A.; Mason, A.; Baker, M. A.; Bettler, D. G.; Changas, A.; McMillen, C. D.; Tapu, D. Janus-type bis(malonhc) and its zwitterionic gold and silver metal complexes. *Organometallics* **2017**, 36, 1867–1872.

(61) Sheldrick, G. M. Crystal structure refinement with shelxl. *Acta Crystallogr. C Struct. Chem.* **2015**, 71, 3–8.

(62) Dolomanov, O. V.; Bourhis, L. J.; Gildea, R. J.; Howard, J. A. K.; Puschmann, H. Olex2: a complete structure solution, refinement and analysis program. *J. Appl. Crystallogr.* **2009**, 42, 339–341.

(63) Spek, A. L. Structure validation in chemical crystallography. *Acta Crystallogr. D Biol. Crystallogr.* **2009**, 65, 148–55.

(64) Bechlars, B.; D'Alessandro, D. M.; Jenkins, D. M.; Iavarone, A. T.; Glover, S. D.; Kubiak, C. P.; Long, J. R. High-spin ground states via electron delocalization in mixed-valence imidazolate-bridged divanadium complexes. *Nat. Chem.* **2010**, 2, 362–8.

(65) Gluyas, J. B. G.; Brown, N. J.; Farmer, J. D.; Low, P. J. Optimised syntheses of the half-sandwich complexes FeCl(dppe)Cp*, FeCl(dppe)Cp, RuCl(dppe)Cp*, and RuCl(dppe)Cp. *Aust. J. Chem.* **2017**, 70, 113–119.

(66) Bruce, M. I.; Ellis, B. G.; Low, P. J.; Skelton, B. W.; White, A. H. Syntheses, structures, and spectro-electrochemistry of {Cp*(PP)Ru}C≡CC≡C{Ru(PP)Cp*} (pp = dppm, dppe) and their mono- and dications. *Organometallics* **2003**, 22, 3184–3198.

(67) Perkins, G. J.; Bruce, M. I.; Skelton, B. W.; White, A. H. A new precursor for organo-osmium complexes. *Inorg. Chim. Acta* **2006**, 359, 2644–2649.

(68) Ohzu, S.; Ishizuka, T.; Kotani, H.; Kojima, T. Reactivity of a Ru(III)-hydroxo complex in substrate oxidation in water. *Chem. Commun.* (*Camb*) **2014**, 50, 15018–21.

(69) Becke, A. D. Density-functional thermochemistry. III. The role of exact exchange. *J. Chem. Phys.* **1993**, 98, 5648–5652.

(70) Hay, P. J.; Wadt, W. R. *Ab initio* effective core potentials for molecular calculations. Potentials for k to Au including the outermost core orbitals. *J. Chem. Phys.* **1985**, 82, 299–310.